# Thermoelastic properties of ringwoodite $(Fe_x,Mg_{1-x})_2SiO_4$: Its relationship to the 520 km seismic discontinuity

Maribel Núñez Valdez [a,*], Zhongqing Wu [b,c], Yonggang G. Yu [c], Justin Revenaugh [d], Renata M. Wentzcovitch [c,e]

[a] School of Physics and Astronomy, University of Minnesota, Minneapolis, MN 55414, USA
[b] School of Earth and Space Sciences, University of Science and Technology of China, Hefei, Anhui 230026, China
[c] Department of Chemical Engineering and Materials Science, University of Minnesota, Minneapolis, MN 55414, USA
[d] Department of Earth Sciences, University of Minnesota, Minneapolis, MN 55414, USA
[e] Minnesota Supercomputing Institute, University of Minnesota, Minneapolis, MN 55414, USA

## ARTICLE INFO

## ABSTRACT

We combine density functional theory (DFT) within the local density approximation (LDA), the quasiharmonic approximation (QHA), and a model vibrational density of states (VDoS) to calculate elastic moduli and sound velocities of $\gamma$-$(Fe_x,Mg_{1-x})_2SiO_4$ (ringwoodite), the most abundant mineral of the lower Earth's transition zone (TZ). Comparison with experimental values at room-temperature and high pressure or ambient-pressure and high temperature shows good agreement with our first-principles findings. Then, we investigate the contrasts associated with the $\beta \rightarrow \gamma(Fe_x,Mg_{1-x})_2SiO_4$ transformation at pressures and temperatures relevant to the TZ. This information offers clearly defined reference values to advance the understanding of the nature of the 520 km seismic discontinuity.

© 2012 Elsevier B.V. All rights reserved.

## 1. Introduction

Wadsleyite ($\beta$-phase) and ringwoodite ($\gamma$-phase) are the high-pressure polymorphs of olivine ($\alpha$-phase), $(Fe_x,Mg_{1-x})SiO_4$. These minerals are the main constituents of the Earth's upper mantle (UM) (Rinwood, 1975; Putnis, 1992) and transition zone (TZ) (Irifune and Ringwood, 1987). Under pressure, the transformation from olivine to wadsleyite happens at $\sim 13.5$ GPa and from wadsleyite to ringwoodite at $\sim 18$ GPa near 1600 K (Katsura and Ito, 1989; Akaogi et al., 1989). These transformations are associated with two major discontinuities in seismic velocities in the Earth's interior at about 410 km and 520 km depth, respectively (Revenaugh and Jordan, 1991). While the first discontinuity is a well characterized and sharp feature in seismic data, the second varies considerably with location.

Experimental and computational approaches have been used to study properties of these minerals at in situ conditions and their relationship with seismic discontinuities. Elasticity and sound velocities of the $\alpha$-$(Fe_x,Mg_{1-x})_2SiO_4$ phase, with $x = 0$–1, have been widely investigated at high pressures and temperatures (see e.g. Núñez Valdez et al., 2010; Stackhouse et al., 2010; Li and Liebermann, 2007, and references therein). On the other hand, even though great efforts have been made to obtain measurements of elastic properties and wave velocities of Fe-free and Fe-bearing wadsleyite and ringwoodite under high temperature and pressure using either ultrasonic or Brillouin scattering techniques (Li et al., 1996; Zha et al., 1997; Isaak et al., 2007; Sinogeikin et al., 1998; Li and Liebermann, 2000; Liu et al., 2009; Mayama et al., 2004, 2005; Isaak et al., 2010; Li, 2003; Higo et al., 2006; Weidner et al., 1984; Sinogeikin et al., 2003; Jackson et al., 2000) results are still limited. Therefore, large extrapolations from room conditions to conditions of the TZ are often used to study this region.

First principles calculations employing the quasiharmonic approximation (QHA), valid up to about two-thirds of the melting temperature, or molecular dynamics (MD) methods, valid near and above melting temperatures, complement each other and are used to obtain elastic moduli under high-pressure–temperature conditions. Calculations of elastic constants using the QHA, though computationally less demanding than MD, still required calculations of vibrational density of states (VDoS) for each strained atomic configuration at several pressures, that is, about 1000 parallel jobs (Da Silveira et al., 2008, 2011).

In this paper we use the analytical and computational approach by Wu and Wentzcovitch (2011) tested only on periclase-MgO, $\alpha$-$Mg_2SiO_4$, and more recently on $\alpha - \beta$-$(Fe_x, Mg_{1-x})_2SiO_4$

* Corresponding author. Tel.: +1 612 624 2872; fax: +1 612 626 7246.
E-mail address: valdez@physics.umn.edu (M. Núñez Valdez).

(Núñez Valdez et al., in press), to calculate bulk ($K$) and shear ($G$) moduli and sound velocities of the $\gamma$-$(Fe_x,Mg_{1-x})_2$ $SiO_4$ phase. This method uses only static elastic constants and phonon density of states for unstrained configurations, therefore reducing the amount of computational time and resources by one to two orders of magnitude. We then address contrasts across the $\beta \rightarrow \gamma(Fe_x,Mg_{1-x})_2 SiO_4$ transition near conditions of the 520 km seismic discontinuity.

## 2. Methodology

### 2.1. Computational details

Calculations based on density functional theory (DFT) (Hohenberg and Kohn, 1964; Kohn and Sham, 1964) were performed using the local density approximation (LDA) (Ceperley and Alder, 1980). This exchange–correlation functional was adopted because it produces the correct orbital occupancy in $(Fe_x,Mg_{1-x})_2$ $SiO_4$ for $x=0.125$ and better structural properties compared to GGA for the Fe-free phase (Yu et al., 2008). Thus, there is no need of LDA+U or GGA/GGA+U for the calculation of structural properties as discussed by Hsu et al. (2011). Ultrasoft pseudopotentials generated by the Vanderbilt method (Vanderbilt, 1990) were used to describe Fe, Si, and O. A norm-conserving pseudopotential generated by the von Car method was used for Mg. Further details about these pseudopotentials are given in Umemoto et al. (2010) and Núñez Valdez et al. (2011). Equilibrium structures of ringwoodite (28 atoms/cell) at arbitrary pressures were found using the variable cell-shape damped molecular dynamics approach (Wentzcovitch, 1991; Wentzcovitch et al., 1993) as implemented in the quantum-ESPRESSO (QE) code (Giannozzi et al., 2009). The plane-wave kinetic energy cutoff used was 40 Ry and for the charge density 160 Ry. The **k**-point sampling of the charge density was determined on a $2 \times 2 \times 2$ Monkhorst–Pack grid of the Brillouin Zone (BZ) shifted by $(\frac{1}{2}\frac{1}{2}\frac{1}{2})$ from the origin. These parameters correspond to having interatomic forces smaller than $10^{-4}$ Ry/a.u. and pressure convergence within 0.5 GPa. Dynamical matrices were obtained using density functional perturbation theory (DFPT) (Baroni et al., 2001). At each pressure, a dynamical matrix was calculated on a $2 \times 2 \times 2$ **q**-point mesh for one atomic configuration only. In principle about 10 other configurations should be used as well, but here we are more interested in the behavior of frequencies with strain and the current approximation seems to be sufficiently accurate. Force constants were extracted and used to compute phonon frequencies in a $12 \times 12 \times 12$ regular **q**-point mesh to produce VDoS.

### 2.2. High-temperature–pressure elastic theory

Exploiting the information about the strain and volume dependence of phonon frequencies, we determine the thermal contribution to the Helmholtz free energy $F$ within the QHA (Wallace, 1972), that is,

$$F(e,V,T) = U_{st}(e,V) + \frac{1}{2}\sum_{\mathbf{q},m} \hbar\omega_{\mathbf{q},m}(e,V)$$
$$+ k_B T \sum_{\mathbf{q},m} \ln\left\{1 - \exp\left[-\frac{\hbar\omega_{\mathbf{q},m}(e,V)}{k_B T}\right]\right\}, \quad (1)$$

where **q** is the phonon wave vector, $m$ is the normal mode index, $T$ is the temperature, $U_{st}$ is the static internal energy at equilibrium volume $V$ under isotropic pressure $P$ and infinitesimal strain $e$, $\hbar$ and $k_B$ are Planck and Boltzmann constants, respectively. Isothermal elastic constants are given by

$$C_{ijkl}^T = \left[\frac{\partial^2 G(P,T)}{\partial e_{ij}\partial e_{kl}}\right]_P, \quad (2)$$

with $G = F + PV$, the Gibbs energy, and $i,j,k,l = 1,\ldots,3$. To convert to adiabatic elastic constants, one uses the relationship

$$C_{ijkl}^S = C_{ijkl}^T + \frac{T}{VC_V}\frac{\partial S}{\partial e_{ij}}\frac{\partial S}{\partial e_{kl}}\delta_{ij}\delta_{kl}, \quad (3)$$

where $C_V$ is heat capacity at constant volume, and $S$ is the entropy. For orthorhombic crystals, the diagonal and off-diagonal elastic constants of Eq. (2) are

$$C_{iijj}^T = \left[\frac{\partial^2 F(\mathbf{e},V,T)}{\partial e_{ii}e_{jj}}\right]_P + (1-\delta_{ij})P(V,T), = C_{iijj}^{st}(V) + C_{iijj}^{ph}(V,T), \quad (4)$$

while the shear elastic constants are

$$C_{ijij}^T = C_{ijij}^{st}(V) + C_{ijij}^{ph}(V,T). \quad (5)$$

The vibrational contribution to the elastic constants, $C_{iijj}^{ph}$ and $C_{ijij}^{ph}$, can be expressed as functions of the volume Grüneisen parameters, $\gamma_{\mathbf{q},m} = -\partial(\ln \omega_{\mathbf{q},m})/\partial(\ln V)$

$$\frac{d\omega_{\mathbf{q},m}}{\omega_{\mathbf{q},m}} = -\gamma_{\mathbf{q},m}\frac{dV}{V}, \quad (6)$$

and their generalization to strain Grüneisen parameters

$$\frac{\partial\omega_{\mathbf{q},m}}{\omega_{\mathbf{q},m}} = -\gamma_{\mathbf{q},m}^{ij}e_{ij}. \quad (7)$$

We have used the Wu–Wentzcovitch method (Wu and Wentzcovitch, 2011) to compute the thermal contribution to the elastic constants, $C_{ijij}^{ph}(V,T)$. This method allows the computation of thermal elastic constants without performing phonon calculations for strained configurations with the approximation that strain and mode Grüneisen parameters have isotropic distributions, which is equivalent to assuming that thermal pressure is isotropic. This is a good approximation (Carrier et al., 2007) implicit in the QHA calculation of thermal pressures.

After obtaining VDoS at several volumes by first principles, average strain Grüneisen parameters were computed at such volumes and interpolated in a fine volume–temperature grid, that was then inverted to a pressure–temperature grid of 0.1 GPa and 10 K spacings. Static elastic constants previously computed (Núñez Valdez et al., 2011) were also used.

Voigt and Reuss bounds of bulk and shear moduli were calculated at high temperature using adiabatic $C_{ij}$, where we omit the superindex $S$ from now on, except when there is place for confusion (Watt et al., 1976; Watt, 1979). With Voight–Reuss–Hill averages of bulk ($K$) and shear ($G$) moduli, isotropic sound velocities were computed as

$$V_P = \sqrt{\frac{K + \frac{4}{3}G}{\rho}}, \quad V_S = \sqrt{\frac{G}{\rho}}, \quad V_\Phi = \sqrt{\frac{K}{\rho}}, \quad (8)$$

where $\rho$ is the density, and $V_P$, $V_S$, and $V_\Phi$ are compressional, shear and bulk velocities, respectively.

## 3. Results

We present here first-principles results of aggregate properties of Fe-bearing ringwoodite at pressures and temperatures relevant to the TZ. All the approximations described in the previous section provided an excellent description of bulk and shear moduli, and sound velocities within the valid regime of the QHA established for the Fe-free quantities (Yu et al., 2008) for $\gamma$-$(Fe_x,Mg_{1-x})_2 SiO_4$ with $x=0$ and $x=0.125$ (see Figs. 1 and 2).

In the case of the Mg-end member ringwoodite, the relationships $dK/dP \gg dG/dP$ and $|dK/dT| > |dG/dT|$ are satisfied in the pressure–temperature intervals considered (Fig. 1a and 2a). At 300 K the agreement between experimental data (Li, 2003;
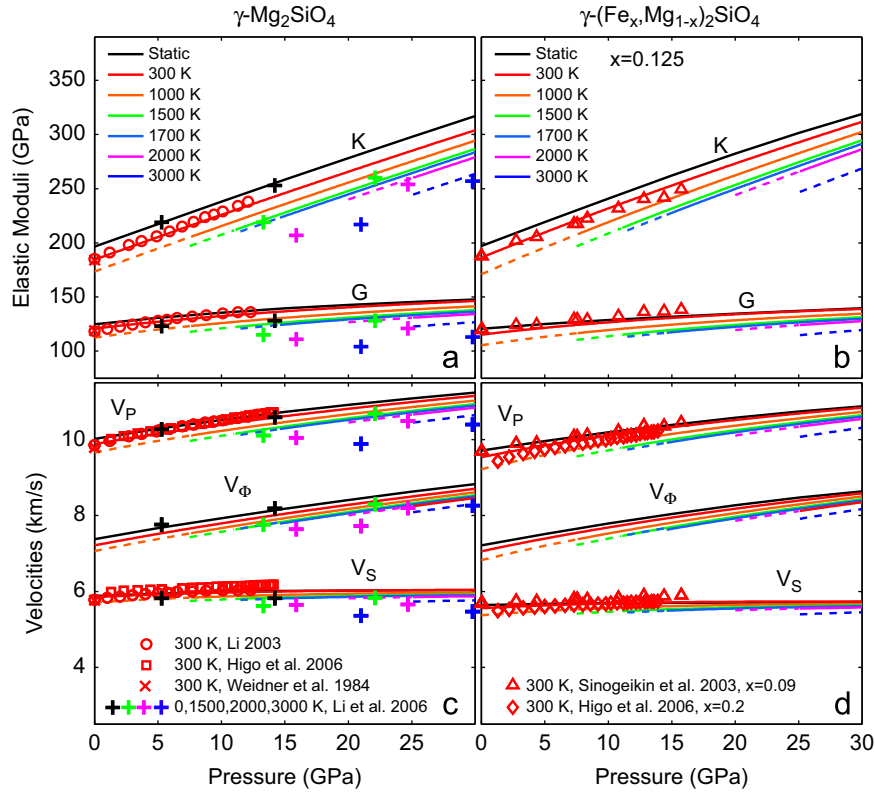
**Fig. 1.** Pressure and temperature dependence of bulk modulus ($K$), shear modulus ($G$), compressional velocity ($V_P$), shear velocity ($V_S$) and bulk velocity ($V_\Phi$) for Fe-free ringwoodite (a,c) and Fe-bearing ringwoodite (b,d). First principles calculations within LDA (solid lines) are compared to available experimental data (symbols). Note, however, that low-pressure–high temperature calculated trends (dash lines) are outside the validity of the QHA.
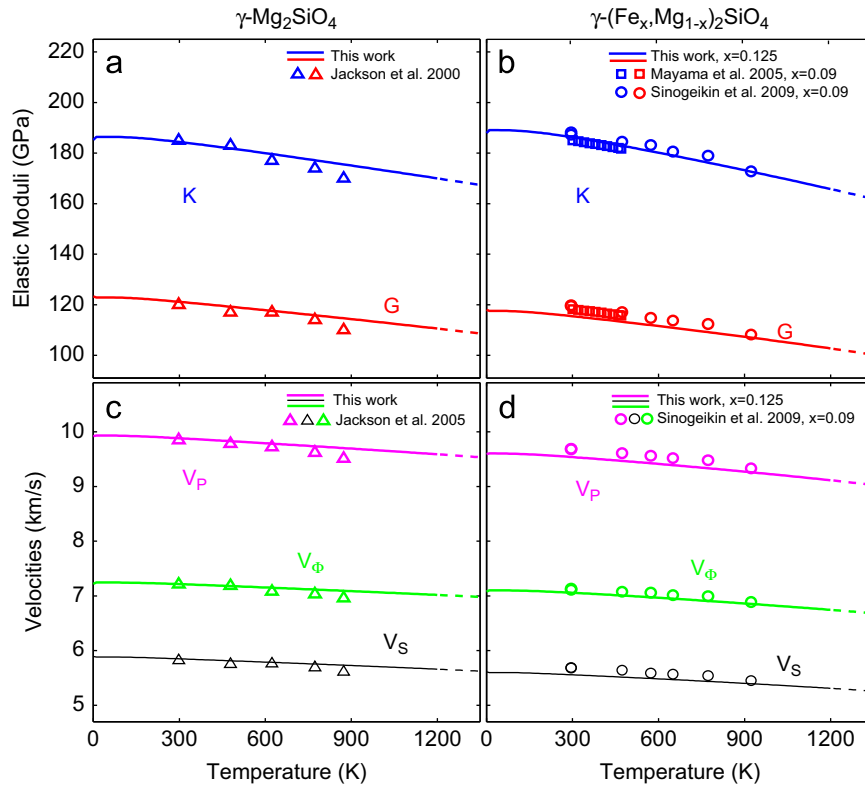


**Fig. 2.** Temperature dependence of bulk modulus ($K$), shear modulus ($G$), compressional velocity ($V_P$), shear velocity ($V_S$) and bulk velocity ($V_\Phi$) for Mg-end member ringwoodite (a,c) and Fe-bearing ringwoodite (b,d). First principles calculations within LDA (solid lines) are compared to available experimental data (symbols) at P=0 GPa.

Higo et al., 2006; Weidner et al., 1984) and our DFT-results is truly excellent for elastic moduli (Fig. 1a), and sound velocities (Fig. 1c). Results from a molecular dynamics study by Li et al. (2006) also compare well with our results for $K$, $V_P$, and $V_\Phi$ within the QHA limits. Our predicted $G$ and $V_S$ are larger and smaller, respectively, than molecular dynamics values (Li et al., 2006). This difference is primarily caused by the use of the GGA approximation in the MD simulation. Nevertheless the general agreement is good and it is the only other source for comparison of aggregate properties of $\gamma$-Mg$_2$SiO$_4$ at high pressures and temperatures. Results of Fe-bearing ringwoodite as a function of pressure are shown in Fig. 1b and d. Experimental data by Sinogeikin et al. (2003) at room temperature and $x=0.09$ are in excellent agreement with our 300 K results for $x=0.125$, though after 10 GPa our $K$ tends to be larger, while $G$ tends to be smaller (Fig. 1b). As expected, Fe-bearing compressional, shear, and bulk velocities are smaller than their Fe-free counterparts (Fig. 1d). Predictions for $x=0.125$ fall in between two experimental reports with iron concentrations of $x=0.09$ (Sinogeikin et al., 2003) and $x=0.2$ (Higo et al., 2006). From Fig. 1d one can see that $V_P$ is the most affected by iron concentration and temperature, while $V_S$ seems to be the least affected by these two factors.

The temperature dependence of elastic moduli and sound velocities of Fe-free and Fe-bearing ringwoodite at ambient pressure are shown in Fig. 2. For $x=0$, the agreement between experimental results (Jackson et al., 2000) and our findings is outstanding (Fig. 2a and c). Similarly, our predicted aggregate properties for $x=0.125$ are in excellent correspondence with experiments for $x=0.09$ (Mayama et al., 2005; Sinogeikin et al., 2003) (Fig. 2b and d). At 300 K, the predicted $K$ increases by $\sim 1\%$ while $G$ decreases by $\sim 4.7\%$ when $x$ changes from 0 to 0.125 (Table 1). But for both moduli, the inequality $|d(K,G)_{x=0}/dT| < |d(K,G)_{x=0.125}/dT|$ is satisfied in the entire 300–1200 K temperature interval. Predicted compressional, shear, and bulk velocities as a function of temperature are smaller than those reported by Sinogeikin et al. (2003), which can be attributed to the difference in iron content (Fig. 2d).

The $x$ dependence of elastic moduli and velocities for $\alpha$-, $\beta$-, and $\gamma$-(Fe$_x$,Mg$_{1-x}$)$_2$SiO$_4$ at high temperatures and pressures is shown in Fig. 3. We find $dK/dx$ to be positive for all three phases, while $dG/dx$, $dV_P/dx$, $dV_S/dx$, and $dV_\Phi/dx$ are negative. For small $x$, a linear trend given by our results of elastic moduli and velocities
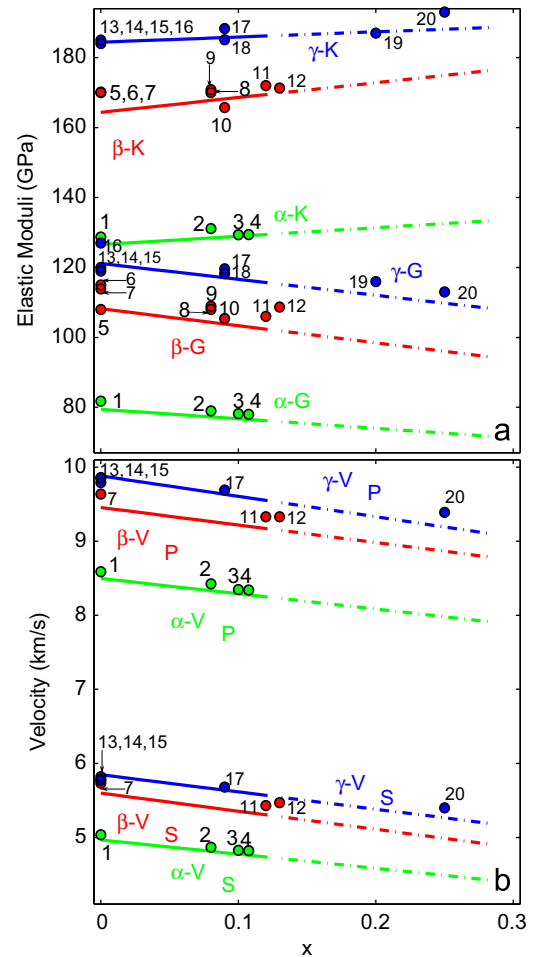


**Fig. 3.** Dependence on low iron content at $P=0$ GPa and $T=300$ K of (a) elastic moduli, $K$ and $G$, and (b) velocities, $V_P$ and $V_S$, (lines) compared to experimental data (circles): 1, Isaak et al. (1989); 2 and 3, Isaak (1992); 4, Abramson et al. (1997); 5, Li et al. (1996); 6, Zha et al. (1997); 7, Isaak et al. (2007); 8, Sinogeikin et al. (1998); 9, Isaak et al. (2010); 10, Mayama et al. (2004); 11, Li and Liebermann (2000); 12, Liu et al. (2009); 13, Weidner et al. (1984); 14, Jackson et al. (2000); 15, Li (2003); 16 and 19, Higo et al. (2006); 17, Sinogeikin et al. (2003); 18, Mayama et al. (2005); 20, Sinogeikin et al. (1997).

**Table 1**
Results on wadsleyite and ringwoodite for volume ($V$), bulk ($K$), and shear ($G$), moduli at ambient pressure and temperature. US: Ultrasonic techniques; BS: Brillouin scattering techniques; RUS: Resonant Ultrasonic techniques.

| $V$ (Å$^3$) | $K$ (GPa) | $G$ (GPa) | $x$ | Reference |
|---|---|---|---|---|
| $\beta$-(Mg$_{1-x}$,Fe$_x$)$_2$SiO$_4$ | | | | |
| 541.3 | 164.4 | 107.7 | 0 | Núñez Valdez et al. (in press), single crystal/DFT |
| – | 170 | 108 | 0 | Li et al. (1996), poly-crystal/US |
| 535.8 (0.2) | 170 (2) | 115 (2) | 0 | Zha et al. (1997), single crystal/BS |
| – | 169.7 (1.9)–170.7 (2) | 113.9 (0.7)–114.1 (0.8) | 0 | Isaak et al. (2007), poly-crystal/RUS |
| 541.5 | 169.5 | 101.7 | 0.125 | This study, single crystal/DFT |
| 539.4 (4) | 170 (3) | 108 (2) | 0.08 | Sinogeikin et al. (1998), single crystal/BS |
| – | 170.8 (1.2) | 108.9 (0.4) | 0.08 | Isaak et al. (2010), poly-crystal/RUS |
| – | 165.72 (6) | 105.43 (2) | 0.09 | Mayama et al. (2004), poly-crystal/RUS |
| – | 172 (2) | 106 (1) | 0.12 | Li and Liebermann (2000), poly-crystal/US |
| – | 171.3 (3) | 108.7 (2) | 0.13 | Liu et al. (2009), poly-crystal/US |
| $\gamma$-(Mg$_{1-x}$,Fe$_x$)$_2$SiO$_4$ | | | | |
| 527.6 | 184.4 | 121.0 | 0 | This study, single crystal/DFT |
| 525.3 | 184 | 119 | 0 | Weidner et al. (1984), single crystal/BS |
| 525.3 | 185 (3) | 120.4 (2) | 0 | Jackson et al. (2000), single crystal/BS |
| – | 185 (2) | 120 (1) | 0 | Li (2003), poly-crystal/US |
| – | 185 (2) | 127 (1) | 0 | Higo et al. (2006), poly-crystal/US |
| 527.7 | 186.3 | 115.3 | 0.125 | This study, single crystal/DFT |
| 526.2 (4) | 188.3 (30) | 119.6 (20) | 0.09 | Sinogeikin et al. (2003), single crystal/BS |
| – | 185.11 (0.16)–185.17 (0.17) | 118.27 (0.06) | 0.09 | Mayama et al. (2005), poly-crystal/RUS |
| – | 187 (2) | 116 (1) | 0.20 | Higo et al. (2006), poly-crystal/US |

compares well to experimental data of olivine and ringwoodite. On the other hand, experimental values of wadsleyite are more scattered and deviate the most from the proposed linear behavior.
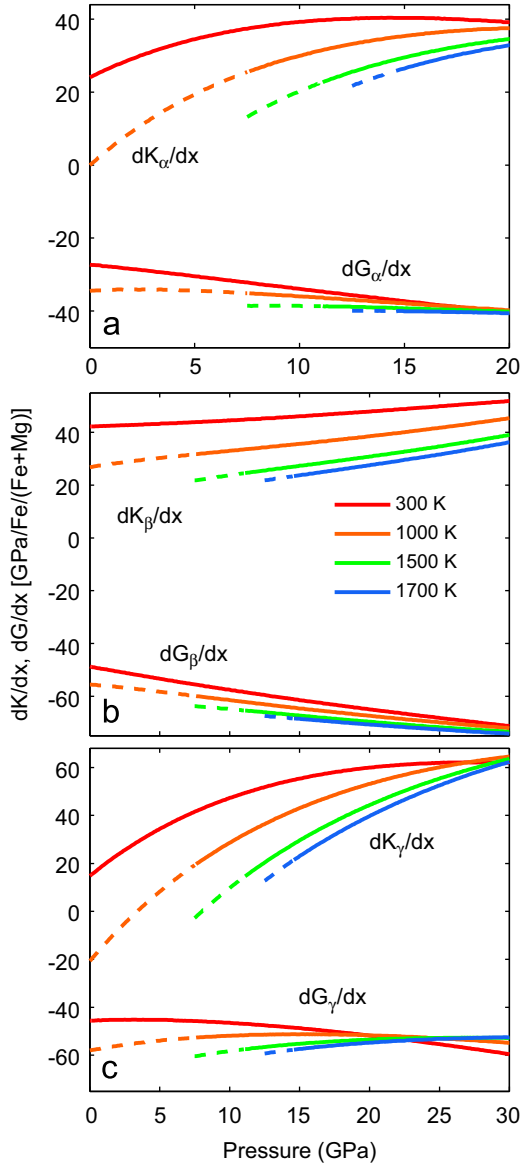


**Fig. 4.** Pressure dependence of $dK/dx$ and $dG/dx$ for (a) olivine, (b) wadsleyite, and (c) ringwoodite.

Detailed dependence on pressure and temperature of $dK/dx$, $dG/dx$, $dV_P/dx$, $dV_S/dx$, and $dV_\Phi/dx$ is shown in Figs. 4 and 5. $dK/dx$ and $dG/dx$ for all three phases exhibit qualitatively similar behavior in the pressure range considered. At low pressure they are quite sensitive to temperature, but they seem to converge at high pressure (Fig. 4a and c). $dV_P/dx$, $dV_S/dx$, and $dV_\Phi/dx$ for all three phases are also more sensitive to temperature at lower pressures.

## 4. Geophysical implications: the 520 km discontinuity

The seismic discontinuity near 520 km depth is often attributed to the phase change of wadsleyite to ringwoodite (Katsura and Ito, 1989; Shearer, 1990; Revenaugh and Jordan, 1991). It is more likely to be unobserved than either of its near neighbors at 410-km and 660-km depth. It is, on average, a smaller amplitude feature (e.g. Revenaugh and Jordan, 1991) such that less frequent observation is to be expected. In some studies the 520 km discontinuity appears as a split arrival or doublet (e.g. Deuss and Woodhouse, 2001; Chambers et al., 2005; Bagley et al., 2009). When split, the two discontinuities are observed at depths of approximately 500 and 560 km (Deuss and Woodhouse, 2001). Notably the sum of the two seismic features is larger than typical non-split observations. Whether this is the result of an upward bias in identifying split arrivals or the result of greater net velocity contrast is not clear. Therefore, accurate data on elasticity of wadsleyite and ringwoodite are critical for investigating the role of the transformation $\beta \to \gamma$ on the 520 km seismic discontinuity.

We use our results on aggregate properties of $\beta$- (Núñez Valdez et al., in press) and $\gamma$-$(Fe_x, Mg_{1-x})_2SiO_4$ at temperatures (1500–1700 K) and pressures (17–19 GPa, $\sim 52$ km width) encompassing the TZ to estimate the magnitude of the discontinuity across the phase transition. Although this is a divariant phase transition and calculation of the two-phase loop is beyond the scope of this work, we can clearly calculate velocity increases throughout the entire transition. As we saw in the previous section, experimental studies dealing with simultaneous high pressures and temperatures offer limited data, and analyses usually extrapolate results at ambient conditions either in temperature or pressure to conditions near 520 km depth ($\sim 18$ GPa and $\sim 1600$ K). The lack of other sources of knowledge makes it difficult to outline conclusions and/or explain the nature of the 520 km seismic discontinuity.

To quantify the magnitude of the discontinuity across the $\beta$ to $\gamma$ transition at finite temperatures we use the contrast $\Delta$ of a particular property $M$ defined as

$$\Delta M = \frac{(M_{x,\gamma} - M_{x,\beta})}{\frac{(M_{x,\beta} + M_{x,\gamma})}{2}} \times 100, \tag{9}$$
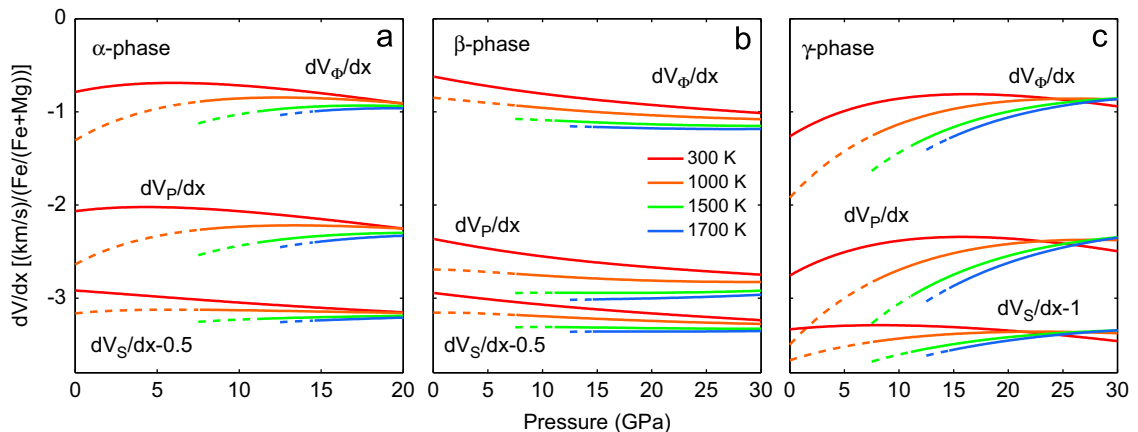


**Fig. 5.** Pressure dependence of $dV/dx$ for (a) olivine, (b) wadsleyite, and (c) ringwoodite.

where $M$ could be density, elastic modulus, or velocity. Table 2 and Fig. 6 show our calculated contrasts at finite temperatures for the $\beta \rightarrow \gamma$ transition in Fe-free and Fe-bearing phases. We first notice that $\Delta \rho$ is almost independent of temperature and pressure with iron having an insignificant effect (Fig. 6a and b), as suggested by Yu et al. (2008). Extrapolated experimental results and seismic data also suggested that iron should have a small effect on this quantity (Rigden et al., 1991; Lawrence and Shearer, 2000; Sinogeikin et al., 2003). Contrasts of elastic moduli (Fig. 6a and b) indicate that $\Delta G$ is more sensitive to temperature than $\Delta K$. This dependence is greater in $x=0.125$ than in $x=0$. As shown in Table 2 and Fig. 6c, velocity contrasts at 18 GPa ($\sim 524$ km depth) for the pure Mg-($\beta \rightarrow \gamma$) transition are predicted to be greater than those given by Rigden et al. (1991, 1992). Based on these results and in the lack of routine observations of a 520 km velocity discontinuity, Shearer (1996) and Lawrence and Shearer (2000) suggested that the shear seismic impedance contrast, $\Delta(\rho V_S) \sim 2.2 - 3.6\%$, occurs mainly because of a change in density rather

than in velocity. Our findings, however, do not support this conclusion. The disagreement could have roots in the fact that measurements by Rigden et al. (1991, 1992) are in the range of 0–3 GPa, and their contrasts are extrapolations to high pressure, while our results are direct calculations at 18 GPa and explicitly account for temperature effects. Our velocity contrasts, across the $\beta \rightarrow \gamma$ transition between 17 and 19 GPa ($\sim 497 - 549$ km depth), are significant and enhanced by Fe-content (Table 2), thus they would be visible in a TZ dominated by (Fe$_x$,Mg$_{1-x}$)$_2$SiO$_4$. Similar results were also found by Sinogeikin et al. (2003) with measurements between 0 and 15 GPa and $x=0.12$. The weakness of the 520 km velocity discontinuity in seismic studies could still be caused by the presence of other phases and water in the TZ, but their effects are not taken into account in this study.

In an attempt to explain the presence of two mid-transition zone discontinuities, Saikia et al. (2008) conducted high pressure (15–24 GPa) and high temperature (1400–1600 °C) experiments to test the solubility of CaSiO$_3$ perovskite in majorite garnet. They concluded that in fertile peridotite (i.e., peridotite enriched in Ca and Al) at 1400 °C, the wadsleyite to ringwoodite phase change produces a strong discontinuity at $\sim 500 - 520$ km depth, while the exsolution of Ca-perovskite produces a weak discontinuity near 540 km. At 1600 °C, the two merge to form a single discontinuity at 540–560 km.

In MORB-like compositions, wadsleyite and ringwoodite are effectively absent, but exsolution of Ca-perovskite causes a velocity discontinuity near 560 km. Saikia et al. (2008) concluded that a mechanical mixture (or seismically averaged assemblage) of peridotite and MORB would have two discontinuities: one near 500 km due to the $\beta$ to $\gamma$ phase change, and a second near 560 km due to the exsolution of Ca-perovskite from garnet, consistent with a hypothesis by Deuss and Woodhouse (2001).

While the transition depths agree with seismic observations, it is less clear that a combination of peridotite and MORB is capable

**Table 2**
Predicted contrasts in % across the $\beta \rightarrow \gamma$-(Mg$_{1-x}$,Fe$_x$)$_2$SiO$_4$ transition at 18 GPa.

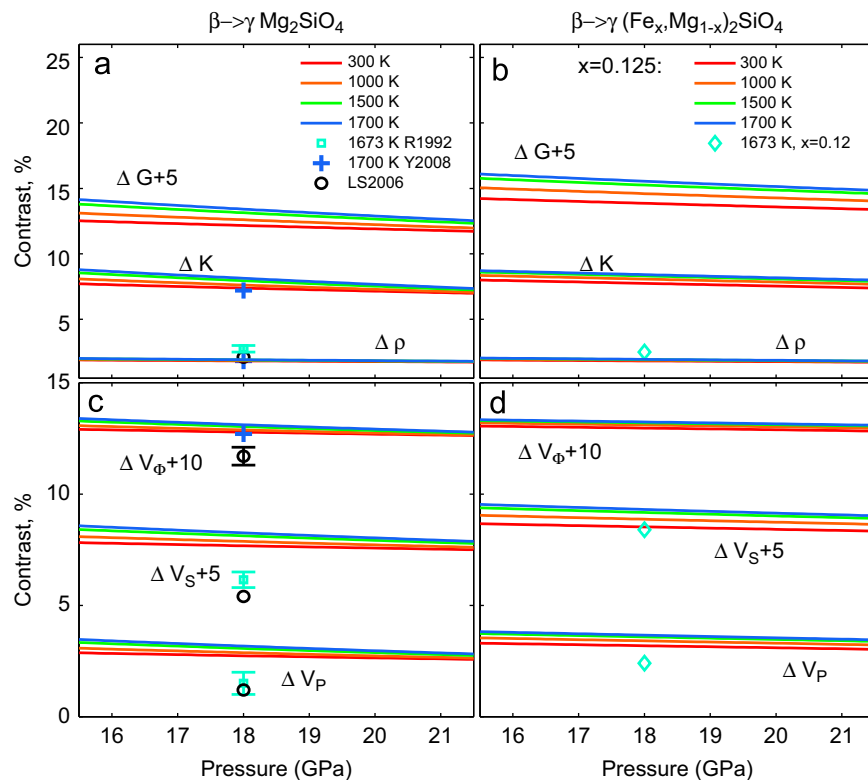| $T$ (K) | 1500 | | 1700 | |
|---|---|---|---|---|
| $x$ | 0.0 | 0.125 | 0.0 | 0.125 |
| $\Delta \rho$ | 1.89 | 1.92 | 1.91 | 1.94 |
| $\Delta K$ | 7.94 | 8.31 | 8.13 | 8.41 |
| $\Delta G$ | 8.14 | 10.26 | 8.42 | 10.55 |
| $\Delta V_P$ | 3.07 | 3.58 | 3.17 | 3.67 |
| $\Delta V_S$ | 3.12 | 4.17 | 3.26 | 4.31 |
| $\Delta V_\Phi$ | 3.03 | 3.20 | 3.11 | 3.23 |
| $\Delta(\rho V_P)$ | 4.96 | 4.99 | 5.08 | 5.11 |
| $\Delta(\rho V_S)$ | 5.02 | 5.04 | 5.17 | 5.20 |



**Fig. 6.** Density, elastic, and velocity contrasts (lines) compared to laboratory and seismic data across the Fe-free (a,c) and Fe-bearing (b,d) $\beta \rightarrow \gamma$ transition. R1992, Rigden et al. (1992); Y2008, Yu et al. (2008); LS2006, Lawrence and Shearer (2000); $x=0.12$, Sinogeikin et al. (2003).

of producing changes in shear velocity and density large enough to match the strengths of the seismic discontinuities. $\Delta V_S$ is a factor of $\sim 2$ lower for the exsolution of Ca-perovskite from majorite garnet in MORB-like material than the wadsleyite to ringwoodite transition (Saikia et al., 2008). Mixing $f$% MORB and $(1-f)$% mantle peridotite to produce the discontinuity doublet reduces the strengths of both discontinuities; by a factor of $f$ ( $<1$ ) for Ca-perovskite exsolution and $(1-f)$ for wadsleyite to ringwoodite. Because the former produces a smaller velocity increase than the latter, the summed velocity change is greatest in a MORB-free mantle ($f=0$), but in this case, there is only a single reflector. However, if the MORB is associated with MORB-depleted mantle (harzburgite or dunite), as might occur if former oceanic lithosphere stagnates in the transition zone, the greater olivine fraction of the depleted mantle results in a seismically stronger (greater $\Delta V_S$) wadsleyite to ringwoodite transition, which would augment the diminished seismic strength of the discontinuity in a depleted mantle–MORB mixture (e.g. Xu et al., 2008). This effect is tempered somewhat by the higher Mg# of basalt-depleted mantle (Jaques and Green, 1980) which we have shown to lower $\Delta V_S$. How strong this effect is depends on the relation between the wadsleyite fraction and Mg# in the depleted mantle which, in turn, depends upon the $P$–$T$ conditions, extent of melting and starting material composition (including volatile components). These complexities make it difficult to precisely estimate the strength of the effect. Nevertheless, the predicted decrease in $\Delta V_S$ and $\Delta V_P$ by higher Mg# of basalt depleted mantle should be considered in future analyses of the single versus the split 520 km discontinuity.

## 5. Conclusions

For the first time, we have presented parameter-free first-principle results of high pressure and high temperature aggregate elastic properties and sound velocities of Fe-bearing ringwoodite. We used the QHA and a novel method of calculating elasticity at high temperatures (Wu and Wentzcovitch, 2011) that exploits isotropic distributions of Grüneisen parameters. This reduced greatly the computational cost of the task, which otherwise would have been much more intensive and lengthy. Within the QHA limit, our predictions for elastic and acoustic properties for $x=0$ were found to be in very good agreement with the available experimental data at 300 K and ambient pressure (Li et al., 1996; Zha et al., 1997; Isaak et al., 2007; Li, 2003; Higo et al., 2006; Weidner et al., 1984) and molecular dynamics simulations (Li et al., 2006) at high pressures and temperatures. For $x=0.125$ our results compared very well with experimental data in the range $x=0.08$–0.2 (Sinogeikin et al., 1998, 2003; Li and Liebermann, 2000; Liu et al., 2009; Higo et al., 2006). High-temperature and ambient pressure results in ringwoodite also reproduced experimental trends very well (Isaak et al., 2007, 2010; Mayama et al., 2004, 2005; Jackson et al., 2000; Sinogeikin et al., 2003) for Fe-free and Fe-bearing samples.

Overall, our predictions showed well-defined changes in the elastic and acoustic properties for the $\beta$- to $\gamma$- phase change near conditions of the 520 km seismic discontinuity. We show that pressure tends to decrease contrasts across the $\beta \rightarrow \gamma$ transition while temperature and iron concentration tend to enhance them. The absence of global observations of the 520 km discontinuity could suggest regions of the TZ with less iron and/or smaller olivine content and irregular temperature topography. Other considerations to try to explain the intermittent nature of the discontinuity would involve changes in the pyroxene/garnet/Ca-pv system and the amount of water present in the TZ. These issues will be addressed in future studies including other relevant phases.

## References

Abramson, E.H., Brown, J.M., Slutsky, L.J., Zaug, J., 1997. The elastic constants of San Carlos olivine to 17 GPa. Geophys. Res. 102, 12253–12263.
Akaogi, M., Ito, E., Navrotsky, A., 1989. Olivine-modified spinel-spinel transitions in the system $Mg_2SiO_4$–$Fe_2SiO_4$: calorimetric measurements, thermochemical calculation, and geophysical application. J. Geophys. Res. 94, 15 671–15 685.
Bagley, B., Courtier, A.M., Revenaugh, J., 2009. Melting in the deep upper mantle oceanward of the Honshu slab. Phys. Earth Planet. Inter. 175 (3–4), 137–144.
Baroni, S., Dal Corso, A., de Gironcoli, S., Gianozzi, P., 2001. Phonons and related crystal properties from density-functional perturbation theory. Rev. Mod. Phys. 73 (2), 515 LP–562 LP.
Carrier, P., Wentzcovitch, R.M., Tsuchiya, J., 2007. First principles prediction of crystal structures at high temperatures using the quasiharmonic approximation. Phys. Rev. B 76, 064116.
Ceperley, D.M., Alder, B.J., 1980. Ground state of the electron gas by a stochastic method. Phys. Rev. Lett. 45, 566–569.
Chambers, K., Deuss, A., Woodhouse, J., 2005. Reactivity of the 410-km discontinuity from PP and SS precursors. J. Geophys. Res. 110 (B2), 1–13.
Da Silveira, P., da Silva, C.R.S., Wentzcovitch, R.M., 2008. Metadata management for distributed first principles calculations in VLab—a collaborative cyberinfrastructure for materials computation. Comput. Phys. Commun. 178, 186.
Da Silveira, P., Núñez Valdez, M., Wentzcovitch, R.M., Pierce, M., Yuen, D.A., 2011. Virtual laboratory for planetary materials (VLab): an updated overview of system service architecture. In: TG'11 Proceedings of the 2011 TeraGrid Conference: Extreme Digital Discovery ACM, New York, NY, USA.
Deuss, A., Woodhouse, J., 2001. Seismic observations of splitting of the mid-transition zone discontinuity in Earth's mantle. Science 294 (5541), 354–357.
Giannozzi, P., et al., 2009. QUANTUM ESPRESSO: a modular and open-source software project for quantum simulations of materials. J. Phys.: Condens. Matter 21, 395502. ⟨http://www.quantum-espresso.org⟩.
Higo, Y., Inoue, T., Li, B., Irifune, T., Liebermann, R.C., 2006. The effect of iron on the elastic properties of ringwoodite at high pressure. Phys. Earth Planet. Inter. 159, 276–285.
Hohenberg, P., Kohn, W., 1964. Inhomogeneous electron gas. Phys. Rev. 136, B864–B871.
Hsu, H., Wentzcovitch, R.M., Umemoto, K., Cococcioni, M., 2011. The Hubbard U correction for iron-bearing minerals: a discussion based on $(Mg,Fe)SiO_3$ perovskite. Phys. Earth Planet. Inter. 185, 13–19.
Irifune, T., Ringwood, A.E., 1987. Phase transformations in primitive MORB and pyrolite compositions to 25 GPa and some geophysical implications. In: Manghnani, M., Syono, Y. (Eds.), High pressure Research in Geophysics. TERRAPUB/AGU. Tokyo, Washington, DC, pp. 231–242.
Isaak, D.G., Anderson, O.L., Goto, T., Suzuk, I., 1989. Elasticity of single-crystal forsterite measured to 1700 K. J. Geophys. Res. 94, 5895–5906.
Isaak, D.G., 1992. High-temperature elasticity of iron-bearing olivines. J. Geophys. Res. 97, 1871–1885.
Isaak, D.G., Gwanmesia, G.D., Falde, D., Davis, M.G., Triplett, R.S., Wang, L., 2007. The elastic properties of $\beta$-$Mg_2SiO_4$ from 295 to 660 K and implications on the composition of Earth's upper mantle. Phys. Earth Planet. Inter. 162, 22–37.
Isaak, D.G., Gwanmesia, G.D., Davis, M.G., Stafford, S.C., Stafford, A.M., Triplett, R.S., 2010. The temperature dependence of the elasticity of Fe-bearing wadsleyite. Phys. Earth Planet. Inter. 182, 107–112.
Jaques, A.L., Green, D.H., 1980. Anhydrous melting of peridotite at 0–15 kb pressure and the genesis of tholeiitic basalts. Contrib. Mineral. Petrol. 73, 287–310.
Jackson, J.M., Sinogeikin, S.V., Bass, J.D., 2000. Sound velocities and elastic properties of $\gamma$-$(Mg_2SiO_4)$ to 873 K by Brillouin spectroscopy. Am. Mineral. 85, 296–303.
Kohn, W., Sham, L.J., 1964. Self-consistent equations including exchange and correlation effects. Phys. Rev. 140, A1133–A1138.
Katsura, T., Ito, E., 1989. The system $Mg_2SiO_4$–$Fe_2SiO_4$ at high pressures and temperatures: precise determination of stabilities of olivine, modified spinel and spinel. J. Geophys. Res. 94, 15,663–15,670.
Lawrence, J.F., Shearer, P.M., 2000. Constraining seismic velocity and density for the mantle transition zone with reflected and transmitted waveforms. Geochem. Geophys. Geosyst. 7, Q10012.
Li, B., Gwanmesia, G.D., Liebermann, R.C., 1996. Sound velocities of Olivine and Beta polymorphs of $Mg_2SiO_4$ at Earth's transition zone pressures. Geophys. Res. Lett. 23, 2259.
Li, B., Liebermann, R.C., 2000. Sound velocities of wadsleyite $\beta$-$(Mg_0.88, Fe_0.12)_2SiO_4$ to 10 GPa. Am- Mineral. 85, 292–295.
Li, B., 2003. Compressional and shear velocities of ringwoodite $\gamma$-$(Mg_2SiO_4$ to 12 GPa. Am. Mineral. 88, 1312–1317.
Li, L., Weidner, D.J., Brotholt, J., Alfè, D., Price, G.D., 2006. Elasticity of $(Mg_2SiO_4)$ ringwoodite at mantle conditions. Phys. Earth Planet. Inter. 157, 181–187.

Li, B., Liebermann, R.C., 2007. Indoor seismology by probing the Earth's interior by using sound velocity measurements at high pressures and temperatures. Proc. Natl. Acad. Sci., 9145–9150.

Liu, W., Kung, J., Li, B., Nishiyma, N., Wang, Y., 2009. Elasticity of $\beta$-$(Mg_0.87,Fe_0.13)_2SiO_4$ wadsleyite to 12 GPa and 1073 K. Phys. Earth Planet. Inter. 174, 98–104.

Mayama, N., Suzuki, I., Saito, T., 2004. Temperature dependence of elastic moduli of $\beta$-$(Mg_{1-x},Fe_x)_2SiO_4$. J. Geophys. Res. 31, L04612.

Mayama, N., Suzuki, I., Saito, T., Ohno, I., Katsura, T., Yoneda, A., 2005. Temperature dependence of elastic moduli of ringwoodite. Phys. Earth Planet. Inter. 148, 353–359.

Núñez Valdez, M., Umemoto, K., Wentzcovitch, R.M., 2010. Fundamentals of elasticity of $(Mg_{1-x},Fe_x)_2SiO_4$-olivine. Geophys. Res. Lett. 37, L14308.

Núñez Valdez, M., da Silveira, P., Wentzcovitch, R.M., 2011. Influence of iron on the elastic properties of wadsleyite and ringwoodite. J. Geophys. Res. 116, B12207.

Núñez Valdez, M., Wu, Z., Yu, Y.G., Wentzcovitch, R.M. Thermoelastic properties of Olivine and Wadsleyite $(Mg_{1-x},Fe_x)_2SiO_4$: their relationship to the 410 km seismic discontinuity. Geophys. Res. Lett., http://arXiv:arxiv.org/abs/1205.4257, in press.

Putnis, A., 1992. Introduction to Mineral Sciences. Cambridge University Press, UK. (399 pp.).

Revenaugh, J., Jordan, T.H., 1991. Mantle layering from ScS reverberations. 2. The Transition zone. J. Geophys. Res. 96, 19,763–19,780.

Rigden, S.M., Gwanmesia, G.D., Fitz Gerald, J.D., Jackson, I., Liebermann, R.C., 1991. Spinel elasticity and seismic structure of the transition zone of the mantle. Nature 354, 143–145.

Rigden, S.M., Gwanmesia, G.D., Jackson, I., Liebermann, R.C., 1992. Progress in high-pressure dependence of elasticity of $Mg_2SiO_4$ polymorphs and constraints on the composition of the transition zone of the Earth's mantle. In: Syono, Y., Manghnani, M.H. (Eds.), High-Pressure Research: Application to Earth and Planetary Science. Geophysical Monograph Series 67, American Geophysical Union, pp. 167–182.

Rinwood, A.E., 1975. Composition an Petrology of the Earth's Mantle. McGraw-Hill, New York. (618 pp.).

Saikia, A., Frost, D.J., Rubie, D.C., 2008. Splitting of the 520-kilometer seismic discontinuity and chemical heterogeneity in the mantle. Science 319 (5869), 1515–1518.

Shearer, P.M., 1990. Seismic imaging of upper-mantle structure with new evidence for a 520-km discontinuity. Nature 344 (6262), 121–126.

Shearer, P.M., 1996. Transition zone velocity gradients and the 520-km discontinuity. J. Geophys. Res. 101 (B2), 3053–3066.

Sinogeikin, S.V., Bass, J.D., Kavner, A., Jeanloz, R., 1997. Elasticity of natural majorite and ringwoodite from the Catherwood meteorite. Geophys. Res. Lett. 24 (24), 3265–3268.

Sinogeikin, S.V., Katsura, T., Bass, J.D., 1998. Sound velocities and elastic properties of Fe-bearing wadsleyite and ringwoodite. J. Geophys. Res. 103 (B9), 20,819–20,825.

Sinogeikin, S.V., Bass, J.D., Katsura, T., 2003. Single-crystal elasticity of ringwoodite to high pressures and high temperatures: implications for 520 km seismic discontinuity. Phys. Earth Planet. Inter. 136, 41–66.

Stackhouse, S., Stixrude, L., Karki, B.B., 2010. Determination of the high-pressure properties of fayalite from first-principles calculations. Earth Planet. Sci. Lett. 289, 449–456.

Umemoto, K., Hsu, H., Wentzcovitch, R.M., 2010. Effect of site degeneracies on the spin crossovers in $(Mg,Fe)SiO_3$ perovskite. Phys. Earth Planet. Inter. 180, 209–214.

Vanderbilt, D., 1990. Soft self-consistent pseudopotentials in a generalized eigenvalue formalism. Phys. Rev. B 41, R7892.

Wallace, D.C., 1972. Thermodynamics of Crystals. John Wiley & Sons, Inc., USA.

Watt, J.P., Davies, G.F., O'Connell, R.J., 1976. The elastic properties of composite materials. Rev. Geophys. Space Phys. 50, 6290–6295.

Watt, J.P., 1979. Hashin–Shtrikman bounds on the effective elastic moduli of polycrystals with orthorhombic symmetry. J. Appl. Phys. 50, 6290–6295.

Weidner, D.J., Sawamoto, H., Sasaki, S., Kumazawa, M., 1984. Single-crystal elastic properties of the spinel phase of $Mg_2SiO_4$. J. Geophys. Res. 89 (B9), 7852–7860.

Wentzcovitch, R.M., 1991. Invariant molecular dynamics approach to structural phase transitions. Phys. Rev. B 44, 2358–2361.

Wentzcovitch, R.M., Martins, J.L., Price, G.D., 1993. Ab initio molecular dynamics with variable cell shape: application to $MgSiO_3$ perovskite. Phys. Rev. Lett. 70, 3947–3950.

Wu, Z., Wentzcovitch, R.M., 2011. Quasiharmonic thermal elasticity of crystals: an analytical approach. Phys. Rev. B 83, 184115.

Xu, W., Lithgow-Bertelloni, C., Stixrude, L., Ritsema, J., 2008. The effect of bulk composition and temperature on mantle seismic structure. Earth Planet. Sci. Lett. 275, 70–79.

Yu, Y., Wu, Z., Wentzcovitch, R.M., 2008. $\alpha \leftrightarrow \beta \leftrightarrow \gamma$ transformations in $Mg_2SiO_4$ in Earth's transition zone. Earth Planet. Sci. Lett. 273, 115–122.

Zha, C.S., Duffy, T.S., Mao, H.W., Downs, R.T., Hemley, R.J., Weidner, D.J., 1997. Single-crystal elasticity of $\beta$-$Mg_2SiO_4$ to the pressure of the 410 km seismic discontinuity in the earth's mantle. Earth Planet. Sci. Lett. 147, E9–E15.